Few-Body Syst (2019) 60:45
https://doi.org/10.1007/s00601-019-1512-1

E. Garrido · **A. S. Jensen**

^{42}Ca and ^{50}Ca with the (Many- and Few-Body) Unified Method

Received: 27 March 2019 / Accepted: 21 May 2019 / Published online: 1 June 2019

Abstract A new method unifying many and few-body aspects of nuclear structure has recently been introduced (Hove et al. in J Phys G Nucl Part Phys 45:073001, 2018). This method combines the many-body description of a core and the few-body structure of this core surrounded by two valence nucleons. For this reason this method is expected to work specially well when applied to nuclei close to the driplines, where the few-body halo structure with one or more nucleons outside the core is established. In this work we apply the new method to nuclei close to the valley of stability, with ^{42}Ca and ^{50}Ca as illustrations. We compare the results from uncorrelated mean-field calculations with the ones obtained with the unified method allowing arbitrary correlations in the valence space. We find that the unified method provides results rather similar, although distinguishable, to the Hartree–Fock calculations. The correlations are much less pronounced than at the driplines, which initially were targets for the unified method. The halo structure is not artificially maintained, but the correlations are here demonstrated to be applicable to well-bound nuclei. Excited states built on valence degrees of freedom are calculated for the same nuclei.

1 Introduction

An appropriate description of the atomic nucleus, which is a complex system made of interacting neutrons and protons, requires a reliable treatment of the corresponding many-body problem [2,3]. One of the simplest methods to do so is the use of a mean-field model, where, by definition, all correlations are neglected [4]. The opposite approach is the interacting shell model, where all correlations are included in the theoretical formulation [5], although severely limited in practice. A large number of different nuclear models are designed and applied to investigate various aspects of the nuclear many-body problem [6–10]. In particular, few-body methods are intended to study relative motion of frozen clusters [11], and the no-core shell model to study nuclear structure materializing at short distance [12].

In classical low-energy nuclear physics the challenge was to account for both collective and single-particle degrees of freedom in the same framework [2]. In modern nuclear structure, this challenge may be similar to incorporating cluster and few-body features in one model. This corresponds to different treatment of intrinsic (short distance) and relative (large distance) cluster degrees of freedom. Recently, such a unified model was

This work was supported by funds provided by the Ministry of Science, Innovation and Universities (Spain) under Contract No. PGC2018-093636-B-100.

This article belongs to the Topical Collection “Ludwig Faddeev Memorial Issue”.

E. Garrido (✉)
Instituto de Estructura de la Materia, CSIC, Serrano 123, 28006 Madrid, Spain
E-mail: e.garrido@csic.es

A. S. Jensen
Department of Physics and Astronomy, Aarhus University, 8000 Aarhus C, Denmark

constructed, where the first formulation uses mean-field approximations and few-body techniques, respectively, for intrinsic and relative cluster degrees of freedom [1]. The applications employed are the Skyrme–Hartree–Fock procedure [4] for one cluster (core), and Faddeev three-body calculations [13] for two surrounding (valence) nucleons.

The traditional few-body techniques have been successfully used to describe cluster nuclei, where nuclear halos at the driplines are perhaps the most obvious examples [14,15]. Reliability of these methods rely on detailed experimental information, which is necessary to construct the phenomenological potentials between intrinsically frozen cluster configurations. The new method has circumvented these problems, first by allowing the core structure to adjust to the influence of the valence nucleons, and second, by using the same nucleon–nucleon interaction between nucleons in the core and between core and valence nucleons [1]. On the other hand, the interaction between valence nucleons must be appropriate for the different Hilbert space allowed for these particles, where variation from in-medium short-distance to large-distance free interaction is necessary.

Successful applications of the unified method on dripline nuclei have already been published. In [16] it is applied to ^{26}O, which is predicted to show a Borromean structure. Also, a good agreement with the experimental invariant mass spectrum after removal of one of the valence neutrons is obtained. This invariant mass spectrum is basically dictated by the derived core–valence neutron interaction, which, once a nucleon–nucleon interaction has been chosen to describe the core, is obtained without any additional free parameter. In [17] the method is applied in the proton dripline region. In particular, the two-proton capture reaction $^{68}\mathrm{Se} + p + p \rightarrow ^{70}\mathrm{Kr} + \gamma$ is considered, the corresponding reaction rates computed, and the capture mechanism investigated. In [18] the emergence of halos and Efimov states is investigated by means of the neutron-rich nucleus ^{72}Ca, showing how the halo configurations emerge from the mean-field structure for three-body binding energy less than $\sim$ 100 keV.

All in all, the unified method has been proved to be efficient in the description of nuclei close the neutron and proton driplines, i.e., in the description of nuclear structures containing loosely bound valence nucleons. However, an aspect still to be tested is how the method performs when applied to nuclei in the valley of stability. At present the core is treated in the mean-field approximation resulting in an uncorrelated structure. Adding two valence nucleons allowed in the full Hilbert space, except the states occupied by identical core nucleons, implies that correlations are possible. The model success at driplines demonstrates that the weakly bound and spatially extended halo-like structures are accounted for.

To investigate different possibilities, we choose two stable well-bound calcium isotopes, ^{42}Ca and ^{50}Ca, where each corresponds to a double magic core (^{40}Ca or ^{48}Ca) plus two additional well-bound neutrons. These configurations seem appropriate as they resemble the cluster structure of a core plus two neutrons assumed in the unified method. The simplifications arise from the empty shells available for the valence nucleons, which simplifies accounting for the Pauli principle.

The paper is organized with Sect. 2 describing the unified model, Sect. 3 presents and discusses the ground state results for the two nuclei, Sect. 4 extends the investigations to excited states of angular momentum higher than zero, and finally, Sect. 5 contains the summary and conclusions.

2 Theoretical Procedure

The starting point of the method used here is to consider the many-body system as a clusterized structure. In this way, the natural choice for the full wave function is the antisymmetrized product of the wave functions describing each of the clusters and a few-body wave function describing their relative motion. This method combines then the many-body description of each individual cluster and the few-body description associated to the relative motion between clusters. We first sketch the method, then focus on the three-body procedure, and last we consider the crucial issue of the Pauli principle.

2.1 Sketch of the Unified Method

The method is described in detail in Ref. [1], and in here we shall concentrate on the practical application to a system formed by a many-body core and two valence nucleons. In this case the full wave function Ψ can be written as:

$$\Psi = \mathcal{A}\left[\psi_c(\{\boldsymbol{r}_c\})\psi_{3b}(\boldsymbol{r}_{cv_1}, \boldsymbol{r}_{cv_2})\right], \tag{1}$$

where $\mathcal{A}$ is the antisymmetrization operator, ψ_c is the wave function of the core that depends on a set of spatial and spin coordinates collected in $\{\boldsymbol{r}_c\}$, and ψ_{3b} is the three-body wave function that depends on the relative coordinates between the core center of mass and the two valence nucleons, $\boldsymbol{r}_{cv_1}$ and $\boldsymbol{r}_{cv_2}$.

In this work the core will be described by means of the Skyrme–Hartree–Fock mean field method [4]. Therefore, the core wave function ψ_c is obtained as the Slater determinant formed by the single-nucleon wave functions $\phi_i^{q_i}$, where i runs over all the nucleons in the core and q_i makes explicit the isospin projection of the nucleon i.

The Hamiltonian, H, and the corresponding interactions are appropriate for Skyrme–Hartree–Fock calculations. The equations of motion are found by minimizing the energy, $E = \langle\Psi|H|\Psi\rangle$, with respect to simultaneous variation of single-particle and three-body wave functions, $\phi_i^{q_i}$ and ψ_{3b}, respectively. The results are a coupled set of equations, that is

$$\begin{aligned}\epsilon_i\phi_i^{q_i}(\boldsymbol{r}) = \Bigg[&-\boldsymbol{\nabla}\cdot\frac{\hbar^2}{2m^*_{q_i}(\boldsymbol{r})}\boldsymbol{\nabla} + U_{q_i}(\boldsymbol{r}) - i\boldsymbol{W}_{q_i}(\boldsymbol{r})\cdot(\boldsymbol{\nabla}\times\boldsymbol{\sigma}) - \\ &-\boldsymbol{\nabla}\cdot\frac{\hbar^2}{2m'^*_{q_i}(\boldsymbol{r})}\boldsymbol{\nabla} + U'_{q_i}(\boldsymbol{r}) - i\boldsymbol{W}'_{q_i}(\boldsymbol{r})\cdot(\boldsymbol{\nabla}\times\boldsymbol{\sigma})\Bigg]\phi_i^{q_i}(\boldsymbol{r}), \qquad (2)\end{aligned}$$

$$\begin{aligned}E_{3b}\Psi_{3b}(\boldsymbol{x},\boldsymbol{y}) = \big[&T_x + T_y + V_{cv_1}(\boldsymbol{r}_{cv_1}) \\ &+ V_{cv_2}(\boldsymbol{r}_{cv_2}) + V_{v_1v_2}(\boldsymbol{r}_{v_1v_2}) + V_{cv_1v_2}(\boldsymbol{r}_{cv_1},\boldsymbol{r}_{cv_2})\big]\Psi_{3b}(\boldsymbol{x},\boldsymbol{y}), \qquad (3)\end{aligned}$$

for the core and valence parts, respectively.

In the Schrödinger-like equation (2), ϵ_i is the single particle energy, $\boldsymbol{\sigma}$ is the usual spin operator, and U_{q_i}, $\boldsymbol{W}_{q_i}$, and $m^*_{q_i}$ are the central and spin–orbit mean-filed potentials, and the effective mass function, respectively. The primed quantities, U'_{q_i}, $\boldsymbol{W}'_{q_i}$, and $m'^*_{q_i}$ are the part of the interaction that arises from the valence nucleon densities. The wave functions of the valence nucleons necessary to construct U'_{q_i}, $\boldsymbol{W}'_{q_i}$, and $m'^*_{q_i}$ are obtained from the three-body wave function ψ_{3b}, see Ref. [1] for details.

The potentials and effective mass are functions of the parameters of the chosen Skyrme interaction and the nuclear densities, which are defined in terms of the single particle functions $\phi_i^{q_i}$ [4,19]. This is the basis of the well-known self-consistent Hartree–Fock method, where some trial single-particle wave functions are used to construct the initial potential and effective mass functions, such that Eq. (2) permits to obtain a new set of single particle functions, which in turn permit to construct new potentials and effective mass. The procedure is iteratively repeated til convergence is reached like solving the usual Hartree–Fock equations [4].

In Eq. (3), E_{3b} is the three-body energy, $\boldsymbol{x}$ and $\boldsymbol{y}$ are the usual Jacobi coordinates, each of them giving rise to the kinetic energy terms T_x and T_y, V_{cv_i} is the interaction between the core and the valence nucleon i, which arises from the mean-field potentials obtained from Eq. (2), and $V_{v_1v_2}$ is the interaction between the two valence nucleons. The vectors $\boldsymbol{r}_{cv_i}$ and $\boldsymbol{r}_{v_1v_2}$ are the relative coordinate between the core center of mass and the valence nucleon i, and the relative distance between the two valence nucleons, respectively. The three-body interaction, $V_{cv_1v_2}$, is used for fine-tuning. The inclusion of such a term is a common feature in standard three-body calculations, where the use of bare two-body interactions typically underbinds the system, [15]. It is designed to describe effects beyond those of the included pair interactions. In the present context this means pieces lost by the density dependent parameterization of the two-body Skyrme interaction. In few-body physics, it accounts for three-body effects of cluster deformation or polarization. Provided that this three-body force has short-range character, its role is basically to shift the energy while maintaining the structure of the system.

The self-consistent practical procedure is now simple. In the initial step we solve the Hartree–Fock equations (2) for the core and obtain an initial core–valence nucleon interaction, which is used in Eq. (3) to obtain an initial three-body solution ψ_{3b}. This wave function is used to construct the valence nucleon single-particle wave functions used in Eq. (2) in order to get a new core–valence nucleon interaction, which in turn is used again in Eq. (3) to get a new three-body wave function and new valence nucleon single-particle wave functions to be used in Eq. (2). The procedure using the output of Eq. (3) as input for Eq. (2), and the output of Eq. (2) as input for Eq. (3) is iterated til convergence is reached.

Both, core and valence structure are influencing each other. The core is only marginally disturbed by the two valence nucleons but still often amounting to a few hundred keV. On the other hand, the valence nucleons are completely controlled by the interaction from the nucleons in the core.

2.2 The Three-Body Calculation

In this work the three-body problem given by the Schrödinger equation (3) will be solved, not actually by solving directly the equation itself, but by solving the Faddeev equations, whose sum provides the Schrödinger equation (3), but which permits a democratic treatment of the internal two-body subsystems. The three-body wave function is written as a sum of three components, each of them depending on each of the three possible sets of Jacobi coordinates, in such a way that each of the three Faddeev equations contains one of the three two-body potentials in its natural coordinate [13].

To be more precise, we shall solve the Faddeev equations in coordinate space by means of the hyperspherical adiabatic expansion method described in [11]. In this method the total three-body wave function is written in terms of the usual hyperspherical coordinates (one radial coordinate, i.e., the hyperradius, and five hyperangles), and it is computed in a two-step procedure. In the first step the hyperradius is considered as a parameter, and the angular eigenvalue problem is solved for fixed values of the hyperradius. The angular eigenfunctions are used as a complete basis set in order to expand the three-body wave function. The radial coefficients in this expansion (functions of the hyperradius) are obtained in a second step as a solution of a coupled set of differential radial equations, where the angular eigenvalues enter as effective (adiabatic) potentials. See Ref. [11] for details.

At this point it is important to mention that the effective mass term, $\hbar^2/(2m^*_{q_i})$, contained in Eq. (2) takes the form $\hbar^2/(2m_{q_i}) - n_a(\boldsymbol{r})$, where m_{q_i} is the constant nucleon mass, and the explicit form of the function n_a can be found for instance in [4]. This fact implies that the interaction V_{cv} between the core and the valence nucleons contains not only the central and spin–orbit parts U_{q_i} and $\boldsymbol{W}_{q_i}$, but also a gradient term of the form $\boldsymbol{\nabla} \cdot n_a(\boldsymbol{r})\boldsymbol{\nabla}$. The presence of this term complicates a little bit the calculation of the three-body wave function. In the particular case of using the adiabatic expansion method, the gradient term in the V_{cv} potential gives rise to a family of new coupling functions in the set of differential radial equations, not described in Ref. [11], but derived in detail in Appendix B of [1].

2.3 The Pauli Principle

The unified method sketched above contains the underlying assumption that the nucleons in the core occupy the lowest possible states, in such a way that only the valence nucleons can move between different orbits. The mean-field calculation used to describe the core guaranties the orthogonality between the different occupied orbits, preventing identical fermions from occupying the same single-particle state in the core.

However, the core–valence nucleon interaction V_{cv_i} generated by the core mean-field is such that the two-body system formed by the core and the valence nucleon shows a series of bound states, each of them with its corresponding ℓ_j quantum numbers, i.e., orbital angular momentum ℓ and total angular momentum j. The important point is that this series of bound two-body states contains all the ℓ_j-states corresponding to the nucleons in the core, therefore already occupied, and forbidden to the valence nucleons by the Pauli principle. It is then clear that these states must be excluded from the space employed when solving the three-body equation (3).

An efficient method to exclude the Pauli forbidden states in the three-body calculation is the use of, not V_{cv_i} as the core–valence nucleon interaction, but of its phase-equivalent version [20]. This amounts to construct a new potential having exactly the same phase shifts as V_{cv_i} for all energies, but whose bound state two-body spectrum does not contain the state(s) forbidden by the Pauli principle.

In the case of using the adiabatic expansion method, a second procedure can also be used in order to exclude the Pauli forbidden states. This method exploits the fact that the effective adiabatic potentials entering in the radial equations are asymptotically associated to specific two-body structures. In particular, some of them will be associated to the Pauli forbidden bound two-body states. The procedure is then simply to exclude these terms from the adiabatic expansion, or, in other words, to exclude the radial differential equations containing the unwanted adiabatic potentials from the set to be solved when computing the radial wave functions [21]. This method is particularly efficient when the adiabatic components to be excluded are, to a large extent, decoupled from the rest. This happens very often with the very deep Pauli forbidden states.

In this work the Pauli principle will be implemented by use of a combination of the two methods described above. If the adiabatic channel associated to a given Pauli forbidden state is very much decoupled from the rest, the second method will be used. Otherwise, we shall construct the corresponding phase equivalent potential. The antisymmetry between core nucleons is then implemented through the Slater determinant, and between valence nucleons directly by using only two-body configurations of the allowed symmetry. But also,

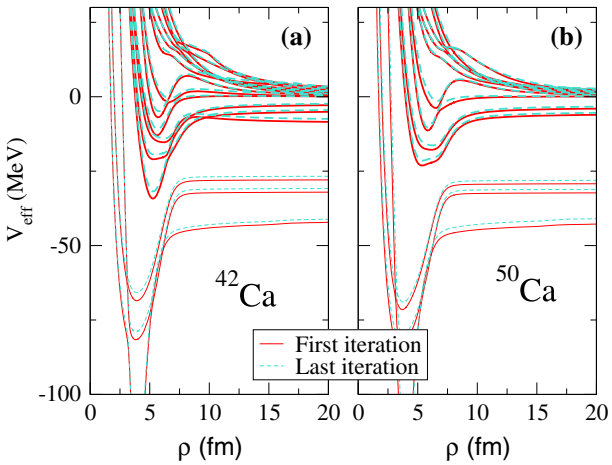

Fig. 1 For ^{42}Ca, panel (**a**), and ^{50}Ca, panel (**b**), three-body effective adiabatic potentials obtained after description of the core by means of the SKM* Skyrme interaction. The solid and dashed curves are the potentials obtained after the first iteration and once the convergence has been reached, respectively. The thin curves correspond to the adiabatic potentials associated to the $1s_{1/2}$, $1p_{3/2}$, and $1p_{1/2}$ Pauli forbidden states that have not been eliminated by means of the phase equivalent potentials

when computing the distorted mean field due to the presence of the valence nucleons, the wave functions of the valence nucleons are antisymmetrized as well with respect to the ones of the nucleons in the core. In other words, across core and valence space, only antisymmetric matrix elements are used in the calculations. Furthermore, only core-unoccupied orbits are allowed for identical valence nucleons.

3 The 0^+ Ground State of ^{42}Ca and ^{50}Ca

We use the unified method to compute the 0^+ ground state of ^{42}Ca and ^{50}Ca as three-body systems of two neutrons surrounding cores of ^{40}Ca and ^{48}Ca, respectively. The self-consistent mean-field calculations provide a sequence of core-occupied single-particle neutron states, that is, with the shell-model notation, the $1s_{1/2}$, $1p_{3/2}$, $1p_{1/2}$, $1d_{5/2}$, $2s_{1/2}$, and $1d_{3/2}$ states, which amounts to the 20 states occupied by the neutrons in ^{40}Ca. These states are Pauli forbidden to the two valence neutrons in ^{42}Ca, which are therefore pushed to the next states, i.e., the $1f_{7/2}$, $2p_{3/2}$, or higher states. In ^{48}Ca also the eight $1f_{7/2}$ neutron states are occupied, and the valence neutrons in ^{50}Ca are pushed to the $2p_{3/2}$ or higher states.

3.1 Effective Three-Body Potentials

The unified method leaves no freedom in the choice of the core–valence nucleon interaction, and as a consequence, the adiabatic potentials entering in the three-body calculation are completely dictated by the chosen effective nucleon–nucleon interaction used to describe the core. The three-body calculations employ the hyperspherical adiabatic expansion method, where we include all partial waves with relative orbital angular momenta up to $\ell = 4$. This amounts to 5 partial waves in the (first) Jacobi set with $\mathbf{x}$ between the two valence neutrons, and 9 partial waves in other two (second and third) identical Jacobi sets. In Fig. 1 we show the effective adiabatic potentials for the 0^+ ground state in ^{42}Ca and ^{50}Ca when the SKM* Skyrme interaction is chosen. The structures are already established after the first iteration (solid curves), which are very similar, although distinguishable, to the converged potentials (dashed curves).

The Pauli forbidden core states have been excluded by use of the corresponding phase equivalent potentials, except for the deep bound states in the s and p-shells. They are seen in Fig. 1 as the three deep states (thin curves) approaching asymptotically at large distance the two-body neutron–core energies around -43 MeV, -32 MeV, and -28 MeV corresponding to the $1s_{1/2}$, $1p_{3/2}$, and $1p_{1/2}$ states. These potentials are, for both nuclei, clearly decoupled from the higher-lying potentials, and they are directly omitted from the subsequent three-body calculation.

Among the remaining potentials (thick curves) in Fig. 1a, still three of them asymptotically approach negative energies at large distance. They correspond to the empty $1f_{7/2}$, $2p_{3/2}$, and $2p_{1/2}$ shells, which

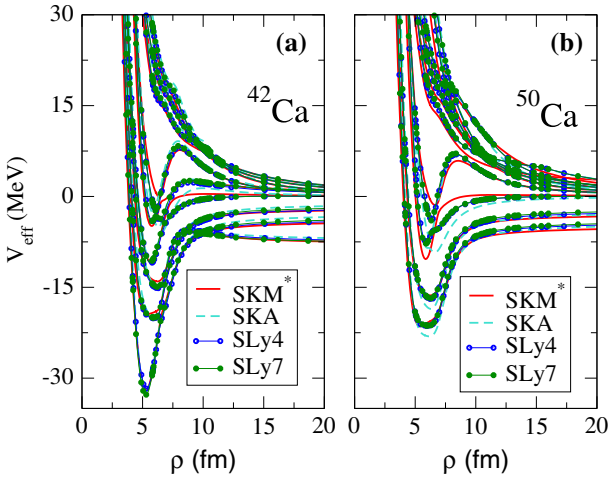

Fig. 2 For ^{42}Ca, panel (**a**), and ^{50}Ca, panel (**b**), converged three-body effective adiabatic potentials obtained after description of the core by means of the SKM*, SKA, SLy4, and SLy7 Skyrme interactions [19]

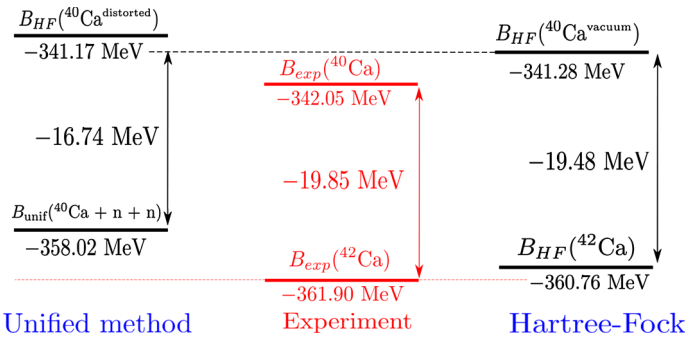

Fig. 3 ^{40}Ca and ^{42}Ca binding energies obtained with the unified method (left) and the Hartree–Fock method (right). The SKM* interaction has been used. The experimental values are given in the central part [23]

therefore are the most likely to be used by the two valence neutrons. For ^{50}Ca in Fig. 1b, only two of them are left with asymptotic negative energies. The third one, corresponding to the $1f_{7/2}$ shell, is now fully occupied by the neutrons in the core, and it has therefore been removed by means of the corresponding phase equivalent potential.

A number of effective interactions are available even for use within the mean-field approximation. To study such uncertainties, we compare in Fig. 2 the decisive adiabatic potentials obtained with four different Skyrme interactions [19]. The differences are minor, and therefore the dependence on the Skyrme interaction is not expected to be significant. We have also compared results from two different neutron–neutron interactions for use entirely within the valence space, the simple Gaussian potential given in [21], and the more sophisticated Argonne v_{18} potential described in [22]. The results again are only marginally different, that is, less 150 keV in the final two-neutron separation energies.

3.2 Energies

The results with the unified method can immediately be compared with pure Hartree–Fock calculations, which are expected to work well for ^{42}Ca and ^{50}Ca, simply because the effective interactions are adjusted to achieve that goal on average for a number of spherical nuclei. The right part of Fig. 3 gives the binding energies of ^{42}Ca and ^{40}Ca obtained in a Hartree–Fock calculation with the SKM* interaction. The difference between these energies is the Hartree–Fock two-neutron separation energy of −19.48 MeV. These results agree reasonably well with the experimental values in the central part of the figure [23]. Both energies are apparently shifted towards less binding by roughly the same amount leaving the two-neutron separation energy almost at the measured value.

Table 1 Two-neutron separation energies, S_{2n}, in MeV for ^{42}Ca and ^{50}Ca, and four different Skyrme interactions

		S_{2n} (MeV)			
		Zero	Conv.	HF (+BCS)	Exp. [23]
^{42}Ca	SKM*	− 18.70	− 16.74	− 19.48(−21.94)	− 19.84
	SLy4	− 17.89	− 16.30	− 18.29(−20.25)	”
	SKa	− 16.99	− 15.68	− 17.70(−20.01)	”
	SLy7	− 18.29	− 16.66	− 18.78(−21.11)	”
^{50}Ca	SKM*	− 11.99	− 10.85	− 12.48(−13.16)	− 11.50
	SLy4	− 10.58	− 9.88	− 10.58(−11.27)	”
	SKa	− 11.00	− 10.41	− 10.90(−11.58)	”
	SLy7	− 10.12	− 9.51	− 10.07(−10.73)	”

The labels “Zero” and “Conv.” refer to our calculation after the initial iteration and after reaching convergence, respectively. The “HF” label refers to the Hartree–Fock calculation. The results within parenthesis are obtained after inclusion of BCS. The experimental data are taken from [23]

The left part of the figure gives the results obtained with the method discussed in this work. This means that the ^{40}Ca core is described after a Hartree–Fock calculation under the presence of the two valence neutrons. This presence is distorting the mean field, which makes the ^{40}Ca core actually slightly less bound than the isolated ^{40}Ca nucleus, due to the distortion away from the optimal configuration. After convergence, we obtain a ^{42}Ca nucleus 2.74 MeV less bound than the pure Hartree–Fock result, leading to the same difference in the two-neutron separation energy. Note that this two-neutron separation energy is taken as the binding energy difference between the computed ^{42}Ca nucleus and the “isolated” ^{40}Ca nucleus. Use of a different Skyrme interaction does not significantly modify the results shown in Fig. 3. The same energies for ^{48}Ca and ^{50}Ca reveal the same qualitative behavior, namely with Hartree–Fock results in reasonable agreement with the experimental values, and with two-neutron separation energies in the vicinity of −11 MeV. Again the unified method gives underbinding for ^{50}Ca by between 0.7 MeV and 2 MeV, depending on the Skyrme force used, compared to the Hartree–Fock calculations.

The summary of the results for the two-neutron separation energies are given in Table 1 for several Skyrme interactions. Under the labels “Zero” and “Conv.” we give, respectively, the computed two-neutron separation energies after the initial iteration and after convergence has been reached. As we can see, right after the first iteration the computed energies are not very different to the ones obtained after a Hartree–Fock calculation (given in the table under the label “HF”). However, as shown in Fig. 1, the iteration procedure, which accounts for the distortion of the core due to the presence of the valence neutrons, gives rise to less deep adiabatic potentials, in such a way that the system becomes less bound than after a Hartree–Fock calculation, as illustrated in Fig. 3.

In the table we also give the results obtained after a Hartree–Fock plus BCS calculation, which improves the agreement with the experimental values. This is not surprising since the pairing strength is chosen phenomenologically to reproduce odd–even differences in average binding energies. However, the unified method does not pick up this pairing effect in energy.

This fact suggests that our interaction between the valence neutrons is too weak in the pairing channel to reproduce the experimental results. The reason can very likely be that the interaction between the valence neutrons used in our calculation is just a free space neutron–neutron interaction [21] (which, as mentioned, provides results very similar to the ones obtained with the Argonne potential [22]). This is necessary with the non-restricted valence Hilbert space, since otherwise the Skyrme zero-range interactions would lead to undesired divergences [1]. The price to pay for this is a poor description of the off-shell (mainly three-body) character of the valence neutrons. Obviously, for nuclei close to the driplines, where the valence neutrons are not that close to the core, the inaccuracy introduced by the use of a bare neutron–neutron interaction is much less pronounced.

Another point to mention here is the effect of the use of phase equivalent potentials in order to eliminate the highest-lying mean-field neutron states forbidden by the Pauli principle. As mentioned, the scattering properties of the new potential are identical to the ones of the original potential, but it has the effect of, first, introducing a repulsion at short distances, and, second, removing one node at small distance in the wave functions available to the valence neutron. This effect, which is also reducing the computed two-neutron separation energy, is clearly largest when the densities at small distances are significant, and, again, it is expected to play a minor role when dealing with nuclei close to the driplines.

Table 2 For four different Skyrme interactions, we give, in fm, the mass root-mean square radii, r_{rms}, of the core, ^{40}Ca and ^{48}Ca, of the full nucleus, ^{42}Ca and ^{50}Ca, and the root-mean square distances between the core and a valence neutron, r_{cn}, and between the two valence neutrons r_{nn}

		^{42}Ca				^{50}Ca			
		SKM*	SLy4	SKa	SLy7	SKM*	SLy4	SKa	SLy7
r_{rms},	Core	3.40	3.40	3.39	3.37	3.55	3.56	3.56	3.54
r_{rms},	Comp.	3.44	3.44	3.44	3.44	3.57	3.58	3.58	3.58
	Comp.+3bd	3.43	3.43	3.43	3.43	3.57	3.57	3.57	3.57
	HF	3.44	3.44	3.43	3.41	3.60	3.61	3.62	3.59
r_{cn},	Comp.	4.12	4.15	4.18	4.12	4.50	4.59	4.61	4.58
	Comp.+3bd	4.09	4.09	4.10	4.07	4.46	4.53	4.54	4.46
	HF	4.06	4.10	4.13	4.07	4.47	4.60	4.66	4.60
r_{nn},	Comp.	5.54	5.58	5.61	5.55	6.02	6.06	6.05	6.04
	Comp.+3bd	5.51	5.50	5.52	5.49	5.97	6.03	5.98	5.95

The label "Comp." refers to our calculation using the unified method, and "Comp.+3bd" refers to our calculation including an effective three-body force such that the experimental two-neutron separation energy is reproduced. The label "HF"' indicates a Hartree–Fock calculation

Summarizing, in the description of well-bound nuclei close to the valley of stability, since the two valence neutrons are relatively close to the core, the use of a free-space neutron–neutron interaction and the use of phase equivalent potentials to take care of the Pauli principle, give rise to a non-negligible underbinding of the system. Close to the driplines, where the valence neutrons are further apart, this problem is much less important. In any case, the underbinding shown in Table 1, although 10−15% in two-neutron separation energy, is less than 1% in the total binding energy.

3.3 Relative Sizes

An indication that the energy differences in Table 1 between our method and the Hartree–Fock method are rather modest, is the fact that the effective three-body force required to fit the experimental value is weak enough to keep the structure of the system essentially unchanged.

The simplest observable revealing structure are the root-mean square radii, which give a measure of the size and the geometry of the system. For the two nuclei and the four Skyrme interactions used in this work, we give in Table 2 several of these second moment expectation values of size measures, that is, the total mass root-mean-square radii (r_{rms}) for the core and the ^{42}Ca and ^{50}Ca nuclei, the distance between the core center-of-mass and one of the valence neutrons (r_{cn}), and the distance between the two valence neutrons (r_{nn}). The label "Comp.+3bd" refers to the result obtained with our method when a three-body force is used to fit the experimental two-neutron separation energy.

The first overall conclusion is that the calculations including the three-body potential are almost identical to those without this force. This is no surprise, rather the intention, by choosing a structureless dependence of the three-body force on only the hyperspherical radius. The combination with rather strong three-body binding results in an approximately constant shift of the potential around its minimum.

The total rms values are not very sensitive to the addition of two valence neutrons, since they are essentially determined by the Hartree–Fock core structure. Comparing r_{cn} in Table 2 from the two methods, we see that the effect of the three-body potential is a small decrease of these radii, which bring them very close to the Hartree–Fock result. These results show that this marginal effect most probably arises from the lowering of the energy, that is moving away from the threshold of no binding.

The average distance between valence neutrons is given by r_{nn}. These radii can be compared to the average distance between nucleons in the core, $r_{cc} \approx r_{rms}\sqrt{2}$, which is roughly the same in the Hartree–Fock treatments of the core and the total system for both ^{42}Ca and ^{50}Ca. The actual core sizes of $3.44(3.57)\sqrt{2} = 4.85(5.03)$ fm are then about 10% (15%) smaller than the computed valence neutron–neutron distances.

The average distance in the unified model from one valence neutron to one nucleon in the core can be estimated as the expectation value of $(\boldsymbol{r}_{nc} - \boldsymbol{r})^2$ over the core distribution with coordinate $\boldsymbol{r}$. For a very heavy core we then get $\sqrt{r_{cn}^2 + r_{rms}^2}$ (since the cross term vanishes after integration), which is, respectively, about 5.3 fm and 5.7 fm. Not surprisingly, these values are between the values of r_{cc} and r_{nn} for the two nuclei.

Table 3 Weight (in %) of the most contributing components to the norm of the ^{42}Ca and ^{50}Ca three-body wave functions. In the notation $(\ell_{x\,j_x}, \ell_{y\,j_y})$ the quantum numbers ℓ_x and ℓ_y are the relative orbital angular momenta between the core and one of the valence neutrons, and between the center of mass of the core–neutron system and second valence neutron, respectively. The coupling between ℓ_x (ℓ_y) and the spin of the first (second) valence neutron provides the angular momentum j_x (j_y)

	^{42}Ca			
	$(f_{7/2}, f_{7/2})$	$(f_{5/2}, f_{5/2})$	$(p_{3/2}, p_{3/2})$	$(p_{1/2}, p_{1/2})$
SKM*	93.7	2.8	1.1	1.1
SLy4	93.8	2.6	1.1	1.1
SKa	94.2	2.5	0.9	0.9
SLy7	94.4	2.5	1.0	0.9
	^{50}Ca			
	$(p_{3/2}, p_{3/2})$	$(p_{1/2}, p_{1/2})$	$(d_{5/2}, d_{5/2})$	$(g_{9/2}, g_{9/2})$
SKM*	95.0	3.2	0.3	0.5
SLy4	94.7	3.5	0.4	0.2
SKa	94.6	3.6	0.3	0.2
SLy7	94.7	3.5	0.4	0.2

These results are consistent with previous results for dripline nuclei [16,18], which is also a reflection of the less restricted Hilbert space in the unified method than in mean-field calculations. This in turn allows the valence neutrons to benefit fully from the largest attraction arising from the core by being far apart if required, perhaps even on opposite sides of the core. The structures in the two methods are very similar but with relatively small differences in striking contrast to the relative sizes found very close to driplines with the halo characteristics. We emphasize that the cluster structure assumed a priory in the unified model has sufficient flexibility to describe continuously uncorrelated mean-field as well as halo structures [1,18].

To further analyze the structure we calculate the partial wave decomposition, shown in Table 3, for the three-body ground state wave functions of ^{42}Ca and ^{50}Ca. Let us take ℓ_x as the relative orbital angular momentum between the core and one of the valence neutrons, and j_x as the coupling between ℓ_x and the spin of the neutron. In the same way, we take ℓ_y as the relative angular momentum between the center of mass of the core–neutron system and second valence neutron, which after coupling to the spin of the second neutron gives the angular momentum j_y.

The two valence neutrons are in pairs of time reversed single-particle states. The weights of the four most contributing $(\ell_{x\,j_x}, \ell_{y\,j_y})$ components to the total norm are given for the ground state wave functions of ^{42}Ca and ^{50}Ca. As expected, for ^{42}Ca the two valence neutrons mainly occupy the $f_{7/2}$ shell, although the three-body calculation predicts small contributions from other two-neutron components, $\sim 2.8\%$ provided by $f_{5/2}$ shell and $\sim 2\%$ by the p shells. The same happens for ^{50}Ca, where the expected structure with the two valence neutrons are moved to higher (but lowest available) shells, that is clearly the $p_{3/2}$ shell dominates with $\sim 95\%$, and contributions of $\sim 3\%$, $\sim 0.35\%$, $\sim 0.3\%$ provided by the shells $p_{1/2}$, $d_{5/2}$ and $g_{9/2}$, respectively.

The linear combination of different configurations is an extension of the Hilbert space used in Hartree–Fock calculations. These admixtures describe correlations beyond mean-field approximations in the few-body wave function and consequently in the total unified wave function. For ^{42}Ca the $f_{5/2}$ states are more favorable than p-states, that is the reversed order compared to the shell model and ordinary Hartree–Fock mean field calculations. This is a signature of the pairing correlation where higher angular momenta are preferred. The arbitrary valence correlations allowed in the unified method is here picking up the pair structure described in the BCS-approximation. The d and g-states from the next major shell are not present, apparently because they would cost too much in energy.

For ^{50}Ca the $f_{5/2}$ state is not contributing although next in the shell model sequence and therefore it should be directly energetic favorable. In contrast, the higher lying (in shell model) d and g-states give visible contributions of the BCS-type of correlations. All these small contributions are significant, at least qualitatively, although most likely sensitive to the angular dependence of the interaction between the valence neutrons.

4 Excited States of ^{42}Ca and ^{50}Ca

The method used here permits as well to compute the excited three-body states arising from the excitation of the valence neutrons. The present method assumes a 0^+ structure for the core, and the total angular momentum

Table 4 Computed, E^*_{comp}, and experimental, E_{exp}, excitation energies, in MeV, of the 2^+, 4^+, and 6^+ excited states in ^{42}Ca, and the 2^+ excited state in ^{50}Ca, arising from the excitation of the valence neutrons

	^{42}Ca			^{50}Ca
	2^+	4^+	6^+	2^+
E^*_{comp}	1.35	1.76	1.43	1.33
E_{exp}	1.52	2.75	3.19	1.03

The experimental values are taken from [23]

has then to be carried entirely by the valence particles. This means that applications are limited to sufficiently low total energies, at least lower than the lowest core excitation energy (3.4 MeV and 3.8 MeV for ^{40}Ca and ^{48}Ca, respectively [23]), where couplings to core excited states are absent or negligibly small.

The j shells mainly occupied by the two valence neutrons can support even angular momentum states from ground state 0^+ to $(2j-1)^+$. We investigate the applicability of the unified method to such states by calculations where the three-body space is restricted to the desired total angular momentum [11]. The dependence on the choice of the Skyrme interaction is very weak for the ground states and we therefore only use one of these interactions, SKM*. We choose again the nuclei ^{42}Ca and ^{50}Ca, and compute excited states with non-zero angular momenta J^π.

An important difference compared to the 0^+ case is that the number of partial waves coupling to the selected total angular momentum is now clearly higher. For instance, for the 2^+ states, if relative angular momenta between the particles up to $\ell = 4$ are included, we get 15 components in the first Jacobi set (5 in the 0^+ case), and 31 in the other two sets (9 in the 0^+ case). This results in much heavier numerical calculations. However, we have observed that the lowest 2^+ states are highly dominated, even by more than 98% of the norm, by the f- and p-wave relative momenta between the core and the valence neutrons for ^{42}Ca and ^{50}Ca, respectively. For this reason, in order to simplify the calculations, the results shown in this section have been obtained including only core–neutron relative f-waves for ^{42}Ca, and only relative p-waves for ^{50}Ca.

We first calculate the 2^+ states whose lowest energies, shown in Table 4, turn out to be 1.35 MeV and 1.33 MeV for ^{42}Ca and ^{50}Ca, respectively. Obviously, different 2^+ states can also be achieved by couplings of a number of other than f and p partial waves, which implies that many 2^+ excited valence states do actually exist, as in fact experimentally observed [23]. Proper comparison to measured spectra then requires detailed structure and decay information, which is beyond the scope of the present paper. We only note here that the computed energies are similar to the energies of the lowest excited 2^+ states present in the measured spectra (1.52 MeV and 1.03 MeV, respectively [23]). For ^{42}Ca, where only relative f-waves between the core and the valence neutrons are included, we observe that the 2^+ state is almost fully dominated by the $(f_{7/2}, f_{7/2})$ configuration, with an almost negligible contribution (less than 1%) from the $(f_{5/2}, f_{5/2})$ and the $(f_{5/2}, f_{7/2})$ components. For ^{50}Ca, about 96% is provided by the $(p_{3/2}, p_{3/2})$ configuration, whereas the remaining 4% is provided by the $(p_{3/2}, p_{1/2})$ component.

There is a number of possible J^π states which can also be achieved by valence excitation. To show the capability and flavor of the unified method, we shall here select a few of such states with the simplest configurations. For ^{42}Ca we extend the sequence of 0^+ and 2^+ to 4^+ and 6^+ states, which are all achieved by the core–neutron f-waves coupling. The energies are also given in Table 4. They are only slightly bigger than the 2^+ energy, and below the experimental values of the lowest 4^+ and 6^+ states [23]. This similarity is perhaps not surprising, since the core is virtually unchanged (less than a few keV variation). Consequently the neutron–core potential is pretty much the same for all angular momenta. In any case, it is important to take into account that the numbers given in Table 4 have been obtained assuming for the 2^+, 4^+ and 6^+ states the same three-body force as the one providing the correct two-neutron separation energy for the ground 0^+ state.

From the wave functions it is also possible to inspect the structure of the different J^π states. We do it with the help of the intrinsic coordinates described in Fig. 4, which are defined after choosing the z-axis along the $\boldsymbol{r}_y$-coordinate (proportional to $\boldsymbol{y}$-Jacobi coordinate) in the second or third Jacobi set. In our case, where the core is 40 or 48 times heavier than the valence particle, the vector $\boldsymbol{r}_y$ can safely be assumed to go from the center of mass of the core to one of the valence neutrons. We then define $r_x^{\parallel}$ and $r_x^{\perp}$ as the projection of $\boldsymbol{r}_x$, which defines the position of the second neutron, along $\boldsymbol{r}_y$ and on the plane perpendicular to $\boldsymbol{r}_y$, respectively. Using now $r_x^{\parallel}$ and $r_x^{\perp}$ as coordinates, it is simple to visualize the position of the second valence neutron relative

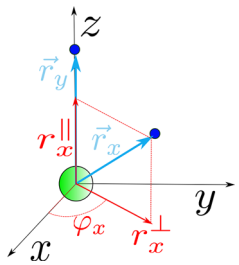

Fig. 4 Definition of the intrinsic coordinates $r_x^{\parallel}$ and $r_x^{\perp}$ in a three-body system where the z-axis is chosen along the Jacobi coordinate $\boldsymbol{y}$ defined between the core and one of the valence neutrons. For ^{42}Ca and ^{50}Ca, whose respective cores are 40 and 48 times heavier than the neutron mass, the $\boldsymbol{y}$-Jacobi coordinate can be, to a large extent, considered as going from the core center of mass to the second valence neutron

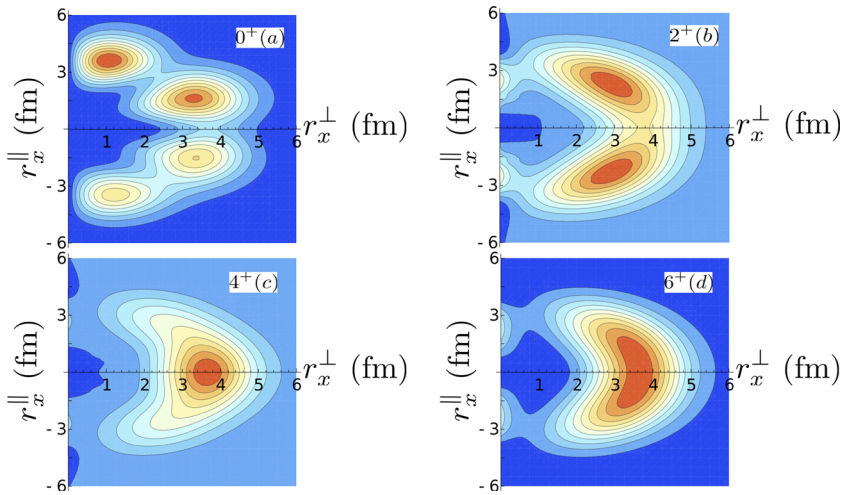

Fig. 5 Contour plots for the intrinsic structure, as defined by the function $\mathcal{F}(r_x^{\parallel}, r_x^{\perp})$ in Eq. (4), for the 0^+, 2^+, 4^+, and 6^+ states in ^{42}Ca. The figures have been obtained using the SKM* interaction

to the first one. We do this with the help of the density function:

$$\mathcal{F}(r_x^{\parallel}, r_x^{\perp}) = \int r_x^{\perp} d\varphi_x d^3 r_y \, |\Psi_{3b}(\boldsymbol{x}, \boldsymbol{y})|^2 \,, \tag{4}$$

where $\Psi_{3b}(\boldsymbol{x}, \boldsymbol{y})$ is the solution of Eq. (3). The function $\mathcal{F}$ is normalized to 1 after integration over $r_x^{\parallel}$ and $r_x^{\perp}$.

The contour plot of the density function (4) is shown in Fig. 5 for the 0^+, 2^+, 4^+, and 6^+ states in ^{42}Ca. The first thing we observe is the symmetry of the function along the $r_x^{\parallel} = 0$ axis. This is a result of the analytical structure of $\mathcal{F}(r_x^{\parallel}, r_x^{\perp})$, from which it is possible to see that when the three-body wave function Ψ_{3b} does not mix even and odd core–neutron relative orbital angular momenta, the equality $\mathcal{F}(r_x^{\parallel}, r_x^{\perp}) = \mathcal{F}(-r_x^{\parallel}, r_x^{\perp})$ is fulfilled. For this reason, since the 2^+, 4^+, and 6^+ states have been obtained including f-waves only, the corresponding density functions are perfectly symmetric along the $r_x^{\parallel} = 0$ axis. For the 0^+ state, the almost negligible contribution from the d-waves is enough to slightly weaken the symmetry along the same axis. The result is that any maximum observed at an angle θ between $\boldsymbol{r}_x$ and $\boldsymbol{r}_y$ in Fig. 4 (an angle θ between the position vectors of the two valence neutrons) has a counterpart at an angle $\pi - \theta$.

As we can see in the figure, even if their excitation energies are not that different, the structure of the four computed states in ^{42}Ca is very different. Four maxima are observed for the 0^+ state and two for the 2^+ state. For the 4^+ and 6^+ states we see that the second neutron has a preference to stay in the plane perpendicular to the direction defined by the first neutron, but even in this case a difference is seen, since in the 6^+ case a deviation from the perpendicular plane is clearly more likely.

5 Summary and Conclusions

In this work we have extended applications of the unified method described in Ref. [1]. The principal virtue of the method is that short- and large-distance properties are directly connected, and both treated in controlled and well-understood approximations. At the moment short distances are described in the mean-field approximation, whereas larger distances are described with state-of-the art methods.

The method assumes a clusterized structure for the nucleus, and the internal many-body cluster degrees of freedom and the few-body relative cluster structure are treated self-consistently. The mean field generated by a given cluster is distorted by the presence of the others, while at the same time determining the cluster-cluster interaction. In other words, the force used in the mean-field calculations also provides by folding the interaction between the clusters. One of the simplest clusterized systems is a many-body core surrounded by a group of valence nucleons. This structure is particularly suitable to describe nuclei close to the proton and neutron driplines, as shown in the previous works [16–18].

In the present work we apply the method to ordinary well-bound nuclei far from the driplines. The purpose is to investigate if the assumed clusterized model structure forces the system to possess the properties characteristic for dripline nuclei. With this main purpose in mind, we have chosen the ^{42}Ca and ^{50}Ca isotopes as an illustration. We have compared the results obtained after pure Hartree–Fock mean field calculations and after use of the unified method describing the system as a ^{40}Ca or ^{48}Ca core plus two valence neutrons.

Four different nucleon–nucleon Skyrme interactions have been used for the Hartree–Fock calculation of the core, as well as for the core–neutron interaction obtained by folding. The Hartree–Fock calculation is done for both core and total nucleus, and the results are very similar for the different interactions. Also the results in the unified method (core with mean-field and valence neutrons with a few-body technique) only weakly depend on the choice of the Skyrme interaction. The latter is seen as the hyperspherical adiabatic potentials entering at the three-body level are very similar, and therefore give rise to correspondingly similar nuclear properties.

More specifically, we considered energies and radii as the characteristic structure properties. The comparison to pure uncorrelated Hartree–Fock results are appropriate, since the unified method introduces correlations in valence space. The unified method with the free-space interaction looses $10-15\%$ in the two-neutron separation energy in comparison with pure Skyrme Hartree–Fock calculations. This is consistent with the typical results obtained after a standard three-body calculation for dripline nuclei, where the system usually is underbound when phase equivalent potentials are used to exclude the Pauli forbidden states. We attribute this result to the combination of neutron–core Skyrme interactions and the unlimited Hilbert space for the valence neutrons with the free-space interaction.

In any case, this difference in the binding energy is not disturbing, since the structure of the strongly bound as well as dripline nuclei are improved. The structure in the unified method remains basically unchanged when the experimental two-neutron separation energy is recovered with an effective three-body force. The substantial benefit is that the new treatment allows correlations between core and valence particles. The structure changes are seen by comparison of relative sizes quantified as second radial moments obtained with the Hartree–Fock and the unified methods. The second moments of two-nucleon distances are rather similar, but the valence distances are significantly larger than both the Hartree–Fock sizes and the corresponding pair distances between core nucleons.

After these ground state calculations we increased the angular momentum to investigate excited states where the core is still angular momentum 0^+, but influenced by the resulting structure of the valence neutrons. For ^{42}Ca the $f_{7/2}$ neutron–core orbit is by far the dominating valence configuration in the ground state, and 2^+, 4^+ and 6^+ states can be formed from the same orbits for two identical nucleons. We approximate for simplicity to only f-partial waves. For ^{50}Ca the dominating valence configurations are p-waves, where only 2^+ states can be formed for identical particles.

The computed excitation energies are in reasonable agreement with the experimental values for the lowest 2^+ states, in both ^{42}Ca and ^{50}Ca, and the lowest 4^+ and 6^+ states for ^{42}Ca , although an unambiguous connection between the computed and measured values would require a more detailed analysis, since many different partial wave configurations can provide the same total angular momentum. We have also shown that the use of the unified method makes accessible the investigation of the spatial structure of the different states. In fact, the computed states in ^{42}Ca, although not very different in energy, show a very different spatial distribution.

In conclusion, the clusterization assumption in the unified method previously used to describe halo structure at driplines, is also applicable to well-bound nuclei close to the valley of stability. Although correlations are

allowed in valence space these well-bound structures are rather similar to those obtained when all core and valence nucleons are treated equally. To have more predictive power for energies, it would be desirable with a better adjustment of the valence interaction to the available space, see [1] for a discussion and an attempt of an answer. This should include special consideration of the pairing channel, which seems so obviously connected to the interaction between the two valence neutrons.

References

1. D. Hove, E. Garrido, P. Sarriguren, D.V. Fedorov, H.O.U. Fynbo, A.S. Jensen, N.T. Zinner, J. Phys. G Nucl. Part. Phys. **45**, 073001 (2018)
2. A. Bohr, B.R. Mottelson, *Nuclear Structure* (Benjamin, Reading, MA, 1969)
3. P.J. Siemens, A.S. Jensen, *Elements of Nuclei* (Addison-Wesley Publishing Company, Redwood City, CA, 1987)
4. D. Vautherin, D.M. Brink, Phys. Rev. C **5**, 626 (1972)
5. E. Caurier et al., Rev. Mod. Phys. **77**, 427 (2005)
6. Y. Kanada-En'yo, H. Horiuchi, Prog. Theor. Phys. Suppl. **142**, 205 (2001)
7. H. Feldmeier, K. Bieler, J. Schnack, Nucl. Phys. A **586**, 493 (1995)
8. M. Hesse, J. Roland, D. Baye, Nucl. Phys. A **709**, 184 (2002)
9. S.K. Bogner, T.T.S. Kuo, A. Schwenk, Phys. Rep. **386**, 1 (2003)
10. H. Hergert et al., Phys. Rep. **621**, 165 (2016)
11. E. Nielsen, D.V. Fedorov, A.S. Jensen, E. Garrido, Phys. Rep. **347**, 373 (2001)
12. B.R. Barrett, P. Navratil, J.P. Vary, Prog. Part. Nucl. **69**, 131 (2013)
13. L.D. Faddeev, Zh Eksp, Teor. Fiz. **39**, 1459 (1961). [Sov. Phys. JETP **12**, 1014 (1961)]
14. A.S. Jensen, K. Riisager, D.V. Fedorov, E. Garrido, Rev. Mod. Phys. **76**, 215 (2004)
15. M.V. Zhukov, B.V. Danilin, D.V. Fedorov, J.M. Bang, I.J. Thompson, J.S. Vaagen, Phys. Rep. **231**, 151 (1993)
16. D. Hove, E. Garrido, P. Sarriguren, D.V. Fedorov, H.O.U. Fynbo, A.S. Jensen, N.T. Zinner, Phys. Rev. C **95**, 061301 (2017)
17. D. Hove, E. Garrido, A.S. Jensen, P. Sarriguren, H.O.U. Fynbo, D.V. Fedorov, N.T. Zinner, Phys. Lett. B **782**, 42 (2018)
18. D. Hove, E. Garrido, P. Sarriguren, D.V. Fedorov, H.O.U. Fynbo, A.S. Jensen, N.T. Zinner, Phys. Rev. Lett. **120**, 052502 (2018)
19. E. Chabanat, R. Bonche, R. Haensel, J. Meyer, R. Schaeffer, Nucl. Phys. A **635**, 231 (1998)
20. E. Garrido, D.V. Fedorov, A.S. Jensen, Nucl. Phys. A **650**, 247 (1999)
21. E. Garrido, D.V. Fedorov, A.S. Jensen, Nucl. Phys. A **617**, 153 (1997)
22. R.B. Wiringa, V.G.J. Stoks, R. Schiavilla, Phys. Rev. C **51**, 38 (1995)
23. R.B. Firestone, S.Y.F. Chu, C.M. Baglin, *Table of Isotopes* (Wiley, New York, 1999)